

Time-Domain Fixed-Structure Closed-Loop Model Identification of an Unstable Multivariable Maglev Nanopositioning System

Huzefa Shakir and Won-jong Kim*

Abstract: This paper presents improved empirical representations of a general class of open-loop unstable systems using closed-loop system identification. A multi-axis magnetic-levitation (maglev) nanopositioning system with an extended translational travel range is used as a test model to verify the closed-loop system-identification method presented in this paper. A closed-loop identification technique employing a known controller structure is used for model identification and validation. Direct and coupling transfer functions (TFs) are then derived from the experimental input-output time sequences and the knowledge of controller dynamics. A persistently excited signal with a bandwidth in the frequency range of interest is used as a reference input. An order-reduction algorithm is developed to obtain TFs with predefined orders, which gives the closest match in the frequency range of interest without missing any significant plant dynamics. The entire analysis is performed in the discrete-time domain in order to avoid any errors due to continuous-to-discrete-time conversion and vice versa. Continuous-time TFs are used only for order-reduction and performance analysis of the identified TFs. Experimental results are presented in the time as well as frequency domains to verify the accuracy of the identified plant TFs. These results also demonstrate the effectiveness of the developed closed-loop identification method in meeting all of the three core objectives—(i) reduction in cross-axial coupling from $9.213 \mu\text{m}$ to $0.911 \mu\text{m}$ in translation and from $22.03 \mu\text{rad}$ to $1.353 \mu\text{rad}$ in rotation, (ii) large range motion capability with a travel range of $\pm 2.9 \text{ mm}$, and (iii) improved robust stability.

Keywords: Closed-loop model identification and validation, magnetic levitation, nanopositioning, order-reduction.

1. INTRODUCTION

Recent developments in the micro- and nanoelectromechanical systems such as precision positioners call for accurate and reliable means of modeling for precise control and manipulation. Some of the major technical challenges that set apart these nanoprecision systems from their macroscale counterparts are added device complexities, nonlinearities and uncertainties present in the system that are hard to detect with conventional methods. An example of significance in this context is the identification and closed-loop control of a maglev system due to its open-loop-unstable dynamics [1]. Following are a few of the major limitations with precision control of this maglev system.

Manuscript received May 13, 2009; revised March 17, 2010; accepted July 3, 2010. Recommended by Editorial Board member Dong Hwan Kim under the direction of Editor Hyun Seok Yang. This material is based upon work supported by the National Science Foundation under Grant No. CMS-0116642.

Huzefa Shakir is with Applied Research Division, Halliburton, 3000 N Sam Houston Pkwy E, Houston, TX 77032, U.S.A. (e-mail: huzefa.shakir@halliburton.com).

Won-jong Kim is with the Department of Mechanical Engineering, Texas A&M University, 3123 TAMU, College Station, TX 77843, U.S.A. (e-mail: wjkim@tamu.edu).

* Corresponding author.

- 1) It generates all the six-axis motions with a single levitated platen. This results in inherent coupling among the axes and thus limits the actual travel range otherwise attainable due to its mechanical design. This problem is more prominent in the extended-range maglev stage since it allows large travel ranges and consequently more coupling.
- 2) One of the control objectives of a maglev system is to have a working space as large as the designed travel range, which implies that the performance of the positioner must be uniform throughout the entire working space. However, the linearized plant model obtained about a specific operating point no longer remains valid and actuator nonlinearities come into play as the deviation of the plant state vector from the operating point increases [1].
- 3) The rotational sensing range of the laser interferometers being used for the horizontal motion sensing is limited to 3.5 mrad . Thus, the cross-talk among the axes may also be responsible for system instability due to loss of sensing data in addition to producing undesired motions.
- 4) The analytical model cannot capture the effect of uncertainties, and unmodeled dynamics due to fabrication and assembly imperfections, and actuator nonlinearities. Modeling these uncertainties analy-

tically can be complicated without perfectly knowing the amount and nature of the imperfections.

These limitations combined with the added design complexity and subnanometer precision requirements call for the development of a modeling technique that is capable of providing better and more accurate plant and cross-coupling models compared to the models obtained by analytical methods with several restrictive assumptions. Accordingly, the main objective of the work presented in this paper is to provide appropriate modifications to the existing model identification and validation methods which often fail to address the practical problems with the underlying assumptions. It is also intended to provide experimental verification of the proposed modifications to demonstrate their use on unstable multi-axis maglev systems to be used as precision positioners.

Model identification is necessary in order to analyze and model the plant dynamics accurately and to subsequently develop effective, reliable, and repeatable control strategies. It is also required to reduce the effect of unmodeled dynamics and nonlinearity in the actuators which may be difficult to model precisely using analytical methods. In the case of a maglev system, this is crucial as well as challenging because of the inherently unstable nature of magnetic levitation [2]. Thus, the system identification needs to be performed in closed loop. Furthermore, due to nonlinearities of the actuators, the linear plant model and controller cannot be used for extended travel range, as the actual force input computed by the controllers based on the larger gaps between the magnet and the coil will be larger than needed and will destabilize the positioner. Therefore, model identification needs to be performed on a small travel range. However, in this case, identification will not capture the nonlinear characteristics of the actuators. An alternative is to use feedback linearization to make the closed-loop system ‘virtually linear’ and then perform the identification on the extended travel range. This method too will not capture the true actuator behavior since we will be deliberately canceling it through feedback linearization.

To handle this problem, we will perform the identification in two steps. In the first step, we will use the feedback linearization together with the linear analytical plant model assumption to stabilize the closed-loop system [1]. Secondly, we perform closed-loop system identification for small-range motion. Finally, we use the identified plant and coupling TF models to design the controllers and retain the use of feedback linearization in hardware-in-the-loop implementation of the controllers for extended-travel-range motion.

Closed-loop model identification has been of particular interest in this context in recent years [3,4]. It is essentially required when a plant is unstable and needs to be stabilized by a feedback controller [5]. There are a few results reported in literature on closed-loop identification. Kuo *et al.* [6] used system identification to validate their proposed mathematical model as well as parameter variations due to changing air gaps for the

ultra-precision motion control of a magnetic-suspension stage. Dejima *et al.* [7] used step responses with a proportional-integral-derivative (PID) control in order to identify the parameters of the plant TF. Villota and Jayasuriya [8] constructed additive uncertainty models by using a zero-mean white-noise random signal as a reference input for system modeling. Lin and Jou [9] developed an improved force-model-identification method for magnetic suspension systems to establish reliable parameters to describe the nonlinear current-to-distance characteristics of the magnetic field. Nakashima *et al.* [10] identified the vibration characteristics of a three-input/output maglev system using closed-loop identification, and designed an \mathcal{H}_∞ servo controller which can effectively suppress these vibrations. A direct closed-loop identification method using the plant input/output data acquired through an output inter-sampling scheme was presented, and its effectiveness was demonstrated through an experimental study using a magnetic-suspension system by Sun *et al.* [4].

As discussed above, a rich prior art is available on a variety of identification methods for different scenarios, some of which are specifically designed for closed-loop system identification. Even though these identification techniques are discussed in elaborate mathematical details, hardly any attention has ever been given in most of the literature on their use in any of the practical applications. Most of the publications are limited to the development of analytical proofs and simulation results at the most. Forsell and Ljung [11], for instance, provided mathematical proof of uniform stability of potentially an open-loop unstable system among others in a closed-loop identification set-up. Likewise, Van den Hof and Schrama [12] revisited identification methods with particular emphasis on closed-loop identification in elaborate mathematical details. While these methods are expected to work perfectly well on any physical system, practical problems often violating one or more of the underlying assumptions, make them susceptible to failure and hence of limited use for practical purposes. Accordingly, the core objective of this paper is to develop an identification method with emphasis on its practical use.

This paper is organized as follows. Section 2 briefly describes the analytical TF model for the maglev positioner. Methods adapted for the model identification and validation will be discussed in Section 3, followed by the detailed algorithm for closed-loop identification. A derivation of the plant and coupling TFs from the identified closed-loop TFs and controller TFs will also be discussed. An order-reduction algorithm will be subsequently presented to get fixed-order TFs in all axes. The identified plant and coupling TFs will be listed and compared to their respective analytical counterparts to demonstrate a close match in the frequency range of interest. Model validation will follow to prove the accuracy of the identified TFs and validate the identification algorithm in the time domain. Important findings in and the significance of this work will finally be summarized in Section 4.

2. ANALYTICAL METHOD

The primary focus of this paper is to present an identification method to estimate the plant parameters of a multivariable open-loop unstable system. Its parameter estimation cannot be performed by using traditional input-output time sequences. Accordingly, the first step is to stabilize the plant in closed loop. In order to demonstrate this, we use a six-degrees-of-freedom (DOF) maglev nanopositioner with open-loop instability, shown in Fig. 1, as a test model. This positioner is based on a novel actuation scheme and is capable of generating all the six-axis motions using minimum number of actuators and sensors. It utilizes a light-weight single-moving platen for positioning with a very simple and compact structure, which gives it an edge over most of the prevailing nanopositioning technologies and allows it to be used as a cluster tool for a variety of applications. Some of these applications are nanoscale lithography, patterning, fabrication, manipulation, and scanning. The maglev positioner operates with a repeatable position resolution of better than 3 nm at the control bandwidth of 110 Hz. It can carry a payload of as much as 0.3 kg and retain the regulated position under abruptly and continuously varying load conditions.

An approximate linearized plant model using analytical method for this system was presented in [13]. To apply the multivariable control, a state-space model of the platen dynamics is required. The plant model was derived using the Newtonian method with the Euler angles. The full equations of motion are nonlinear because of the dependence of motion of the platen on the trigonometric functions of the angles of rotation with respect to the inertial frame. These equations for lateral motion of the platen are given by [13]

$$\dot{\tilde{x}} = u, \quad (1)$$

$$\dot{\tilde{y}} = v, \quad (2)$$

$$\dot{\tilde{\phi}} = \frac{\sin \psi}{\cos \theta} q' + \frac{\cos \psi}{\cos \theta} r', \quad (3)$$

$$\dot{\tilde{u}} = \frac{1}{m} \begin{bmatrix} f_x (\cos \theta \cos \phi) \\ + f_y (\sin \psi \sin \theta \cos \phi - \cos \psi \sin \phi) \\ + f_z (\cos \psi \sin \theta \cos \phi + \sin \psi \sin \phi) \end{bmatrix}, \quad (4)$$

$$\dot{\tilde{v}} = \frac{1}{m} \begin{bmatrix} f_x (\cos \theta \sin \phi) \\ + f_y (\sin \psi \sin \theta \sin \phi + \cos \psi \cos \phi) \\ + f_z (\cos \psi \sin \theta \sin \phi - \sin \psi \cos \phi) \end{bmatrix}, \quad (5)$$

$$\dot{\tilde{r}}' = \frac{1}{I_{zz}} \begin{bmatrix} -\tau_x \sin \theta + \tau_y \sin \psi \cos \theta + \tau_z \cos \psi \cos \theta \end{bmatrix}. \quad (6)$$

The linearized plant model equation in the state-space matrix form for optimal multiple-input-multiple-output (MIMO) controller design with the state vector $[\tilde{x}, \tilde{y}, \tilde{\phi}, \dot{\tilde{x}}, \dot{\tilde{y}}, \dot{\tilde{\phi}}]$ is given by

$$\begin{bmatrix} \tilde{X}(s) \\ \tilde{Y}(s) \\ \tilde{\Phi}(s) \end{bmatrix} = \begin{bmatrix} \frac{1}{ms^2} & 0 & 0 \\ 0 & \frac{1}{ms^2} & 0 \\ 0 & 0 & \frac{1}{I_{zz}s^2} \end{bmatrix} \begin{bmatrix} \tilde{F}_x(s) \\ \tilde{F}_y(s) \\ \tilde{T}_\phi(s) \end{bmatrix}. \quad (7)$$

The general form of this dynamic model with the inclusion of cross-axial coupling TFs and output noises may be represented as

$$\begin{bmatrix} \tilde{X}(s) \\ \tilde{Y}(s) \\ \tilde{\Phi}(s) \end{bmatrix} = \begin{bmatrix} G_{xx}(s) & G_{yx}(s) & G_{\phi x}(s) \\ G_{xy}(s) & G_{yy}(s) & G_{\phi y}(s) \\ G_{x\phi}(s) & G_{y\phi}(s) & G_{\phi\phi}(s) \end{bmatrix} \begin{bmatrix} \tilde{F}_x(s) \\ \tilde{F}_y(s) \\ \tilde{T}_\phi(s) \end{bmatrix} + \begin{bmatrix} H_x(s) & 0 & 0 \\ 0 & H_y(s) & 0 \\ 0 & 0 & H_\phi(s) \end{bmatrix} \begin{bmatrix} E_x(s) \\ E_y(s) \\ E_\phi(s) \end{bmatrix}, \quad (8)$$

where $\tilde{X}(s)$, $\tilde{Y}(s)$, and $\tilde{\Phi}(s)$ are the Laplace transforms of the perturbations of the horizontal positions and the yaw angle from their respective operating points; $\tilde{F}_x(s)$, $\tilde{F}_y(s)$, and $\tilde{T}_\phi(s)$ are the respective plant inputs as forces and torque; $E_x(s)$, $E_y(s)$, and $E_\phi(s)$ are the output noises; and $G(s)$ and $H(s)$ are plant and noise TFs, respectively. The axis convention and assembly of the maglev positioner is shown in Fig. 1. The force transformation between the modal forces $[f_x, f_y, \tau_\phi]$, and the actuator forces $[F_1, F_2, F_3]$ is given by

$$\begin{bmatrix} f_x \\ f_y \\ \tau_\phi \end{bmatrix} = \begin{bmatrix} 0 & \sqrt{3}/2 & -\sqrt{3}/2 \\ -1 & 1/2 & 1/2 \\ -l & -l & -l \end{bmatrix} \begin{bmatrix} F_1 \\ F_2 \\ F_3 \end{bmatrix}, \quad (9)$$

where l is the distance between the point of application of the actuator forces and the center of the maglev moving platen. Since the platen is suspended without any

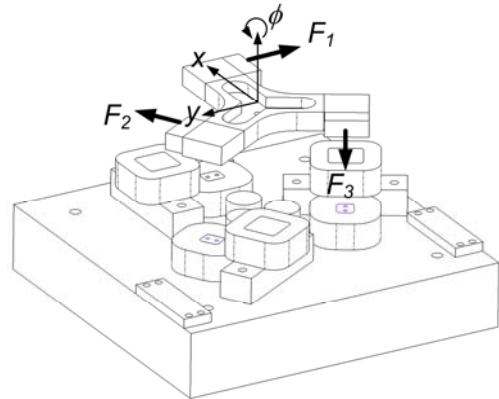


Fig. 1. Axis convention and assembly structure of the maglev positioner [1].

mechanical contact, the plant model can be thought of as a pure mass accelerating with the application of electromagnetic forces. Thus in an ideal linearized dynamic model, each diagonal term of the plant TF matrix could be considered as a double integrator,

$$G_{xx}(s) = G_{yy}(s) = \frac{1}{ms^2}, \quad G_{\phi\phi}(s) = \frac{1}{I_{zz}s^2}, \quad (10)$$

where m is the mass of the platen and I_{zz} is its principal moment of inertia about the z -axis. The off-diagonal terms and noise TF terms might be ignored in an ideal model.

3. CLOSED-LOOP SYSTEM IDENTIFICATION

This section describes the methodology adapted for the closed-loop system identification, the order-reduction algorithm to get fixed-order TFs, and the model validation in the frequency as well as time domains, together with physical interpretations of the identified models. Fig. 2 shows the steps involved in the identification and validation methods. These methods will now be discussed in detail.

3.1. Methodology

System identification is required to validate the analytical model (8)-(10) and to identify the dynamic coupling among the axes due to the non-ideal actuators and mechanical structure of the positioner, and misalignments in its assembly. Open-loop tests cannot be performed due to the inherently unstable nature of the maglev system [2]. Subsequently, the identification of the experimental system is carried out on the closed-loop system after the maglev positioner is stabilized about the operating point with a known decentralized controller in each DOF [14,15]. The schematic of this method is shown in Fig. 3. Since the system-identification procedure is carried out in discrete time, the continuous-time model in (8) was transformed into difference equations using the zero-order-hold (ZOH) method with a sampling frequency of 5 kHz. For example, the discrete-time TF equation for x , under certain assumptions [14,15], is given by

$$\begin{aligned} \tilde{X}(k) &= \frac{B_x(q)}{A_x(q)} R_x(k) + \frac{C_x(q)}{D_x(q)} E_x(k) \\ &\quad + f(G_{yx}(q), M_x(q)) R_y(k) \\ &\quad + f(G_{\phi x}(q), M_x(q)) R_\phi(k) \\ &= \frac{G_{xx}(q) M_x(q)}{1 + G_{xx}(q) M_x(q)} R_x(k) \\ &\quad + \frac{H_x(q)}{1 + G_{xx}(q) M_x(q)} E_x(k) \\ &\quad + f(G_{yx}(q), M_x(q)) R_y(k) \\ &\quad + f(G_{\phi x}(q), M_x(q)) R_\phi(k), \end{aligned} \quad (11)$$

where $G(q)$, $H(q)$, and $M(q)$ are rational TFs, $R(k)$ is the reference input signal, $M(q)$ is the known controller TF,

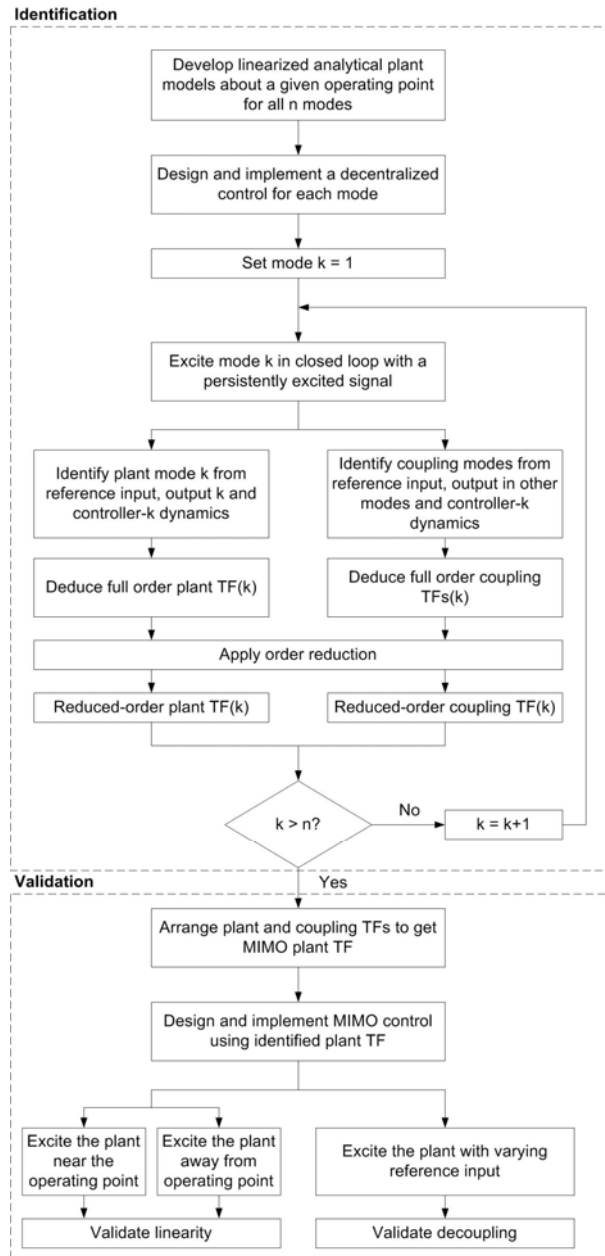


Fig. 2. Flow chart describing the major steps involved in the model identification and validation methods for an unstable multivariable system.

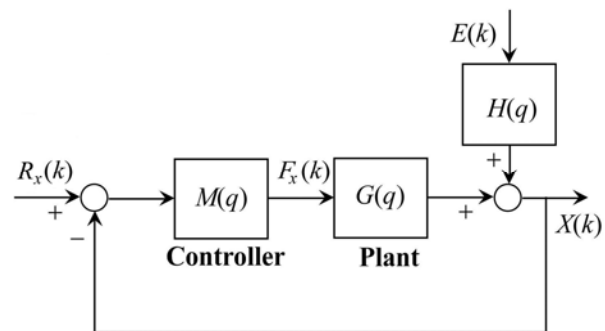


Fig. 3. Block diagram representing the schematic used for identification in closed loop with known controller dynamics.

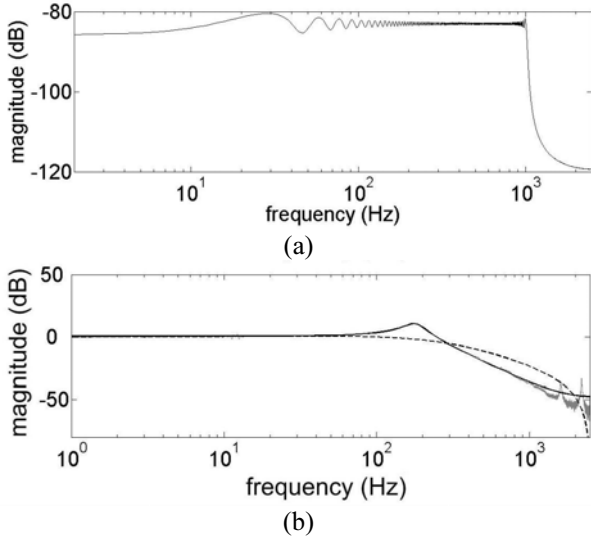


Fig. 4. (a) Frequency response of a chirp signal with frequencies from 0 to 2500 Hz used as a reference input for closed-loop system identification, and (b) closed-loop system frequency response in x to this input signal with Bode magnitude plots of the analytical model (dashed line), the plant TFs from the fast Fourier transforms (FFTs) of the input-output signals (thin solid lines), and the identified TFs using the closed-loop system identification (thick solid lines).

and $q = z^{-1}$. When we identify $G_{xz}(q)$, $R_y(k)$ and $R_\phi(k)$ are set to zero. Due to the chosen structure for the parameterization of the plant and noise models, the TFs $G(q)$ and $H(q)$ are parameterized independently. The relations for identification of the coupling TFs may be similarly written using $G_{yx}(q)$ and $G_{\phi x}(q)$.

Since we have full control over the excitation signal, it is desirable to use the signals that persistently excite the plant [15]. Furthermore, deterministic signals give

cleaner estimates of transfer functions compared to the random ones [16]. Thus, the model identification was performed with a chirp signal. In this experiment, we used chirp signal with a magnitude of $1 \mu\text{m}$, starting from DC and crossing 2500 Hz at 2 s. These numbers were chosen to excite the plant persistently without losing the closed-loop system stability. The total time of the excitation was 2 s with a sampling rate of 5 kHz. The experimental results of the system identification are presented in Fig. 4. The frequency response of the input signal is shown in Fig. 4(a). Fig. 4(b) shows the closed-loop frequency response of the reference input signal, the identified TF, and the ideal closed-loop TF.

Fig. 5(a) shows the $1\text{-}\mu\text{m}$ -amplitude chirp signal given in x , with its frequencies in the range of $[0, 2500]$ Hz and the response of the closed-loop system in x , y , and ϕ . The total time of excitation was 2 s. Figs. 5(b) and 5(c) show similar plots with excitation in y and ϕ , the responses in the respective axes and the coupled responses. It may be seen from these plots that the plant follows the chirp signal closely in the low-frequency range, around $[0, 50]$ Hz. It, however, amplifies the input in the intermediate-frequency range, and attenuates, in the high-frequency range. This is in agreement with the closed-loop TF identified in Fig. 4(b), which exhibits a resonance in the frequency range of $[50, 250]$ Hz and a steep roll-off thereafter.

From Figs. 5(a) and 5(b) the coupling in x with excitation in y is more conspicuous compared to that in y with excitation in x . This may be attributed to the fact that the y -component of the forces F_5 and F_6 , which gets canceled to generate an effective motion in x are smaller ($1/2\times$), whereas the canceling x -components for a desired effective motion in y come from the larger ($\sqrt{3}/2\times$) components of the forces F_5 and F_6 (refer to (9) for details on force transformation). Therefore, if there is any net non-zero force in the coupled axes due to misalignments or modeling uncertainties, the effect of

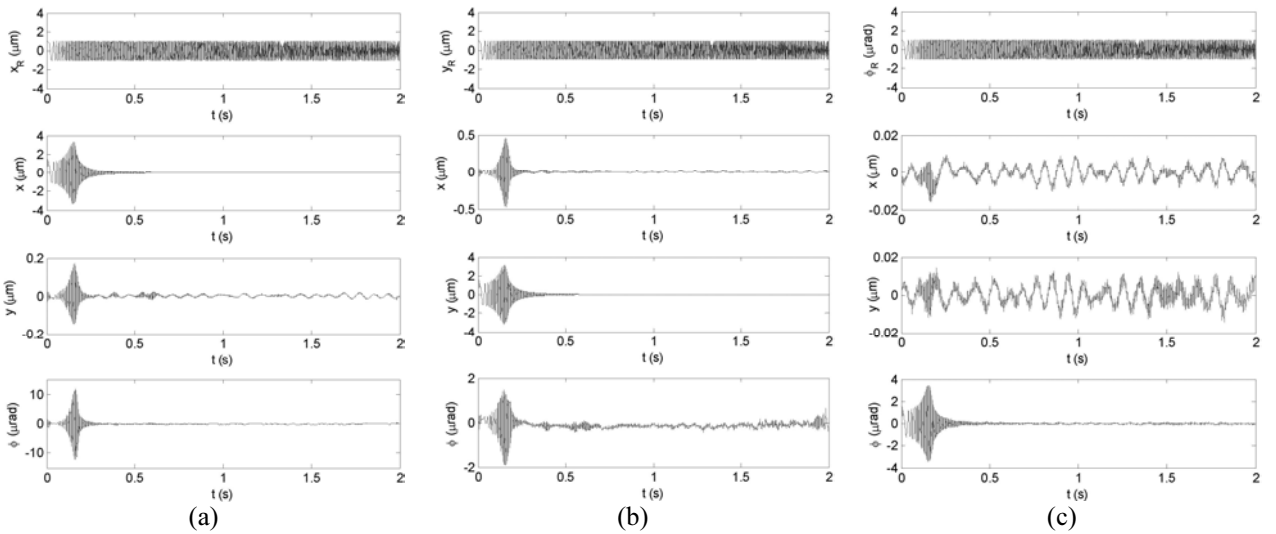


Fig. 5. Closed-loop system time responses to a chirp signal in (a) x , (b) y , and (c) ϕ in the frequency range of $[0, 2500]$ Hz with coupled responses in other axes.

such a force will be more prominent in x compared to y . On the other hand, the coupling in ϕ is greater with excitation in x compared to excitation in y . The reason for this may be explained as follows. The amount of canceling forces in ϕ is the same for both the cases. However, in case of x , components from two forces, namely F_5 and F_6 , get canceled, while in case of y , components from F_4 , F_5 , and F_6 get canceled (refer to (9)). Therefore, if there is any misalignment in the actuators or position of the maglev stage with respect to the actuators, the effect of such misalignments and modeling uncertainties will be averaged over two forces in case of x while three forces in case of y . Accordingly, the net coupling will be less in case of the y -excitation. Finally, from Fig. 5(c), the coupling in x and y is minimal with excitation in ϕ , and the responses in these two axes are almost the same as that of position regulation. For further details on the force generation by the actuators for 6-DOF motion, the reader is referred to [1]. This comparison will be discussed in more detail in terms of the frequency response, and plant and coupling TFs in Section 3.3.

3.2. Closed-loop identification algorithm

With the reference input signals in the three axes and measured output signals in the respective axes as well as coupled axes, all nine TFs of the TF matrix in (8) can be identified. Model identification was performed with MATLAB using an algorithm consisting of the following steps.

3.2.1 Identification of closed-loop plant and coupling TFs

In this step, the parameters of the polynomials A , B , C , and D given in (11) are identified. Identification is performed using the following model structure [15].

$$F(q)X(k) = \frac{B(q)}{A(q)}R(k - n_k) + \frac{C(q)}{D(q)}E(k). \quad (12)$$

Note that (11) is a special case of the general structure given by (12). Also note that the signal-to-noise ratio in the above-mentioned experiments was experimentally determined to be about 80 dB and was found to be frequency-independent. Thus the contribution from the sensor noise $E(k)$ in (11) may be ignored although it is not difficult to determine the noise TFs $H(q)$ together with the plant TFs from the closed-loop input-output sequences.

Identification was performed using iterative prediction-error minimization method. The estimation method is similar to auto-regressive moving average with exogenous input (ARMAX) method and uses optimization to minimize the cost function, defined as follows for scalar outputs.

$$V_N(G, H) = \sum_{t=1}^N e^2(t), \quad (13)$$

where $e(t)$ is the difference between the measured output

and the predicted output of the model. For a linear model, this error is defined by the following equation

$$e(t) = H^{-1}(q)[x(t) - G(q)r(t)]. \quad (14)$$

The subscript N indicates that the cost function is a function of the number of data samples and becomes more accurate for larger values of N . The estimation was performed using MATLAB.

Let us now define the closed-loop TF as $T(q)$, where

$$T(q) = \frac{G(q)M(q)}{1 + G(q)M(q)} = \frac{B(q)}{A(q)}. \quad (15)$$

Here the subscripts used in (11) were dropped for simplicity. Let $[n_G^c, d_G^c]$ and $[n_M^c, d_M^c]$ be the orders of the numerator and denominator polynomials of the continuous-time plant and controller TFs, respectively. Then, from the analytical plant model given by (10) and the stabilizing lead-lag controller design, we have

$$\begin{aligned} [n_G^c, d_G^c] &= [0, 2], \\ [n_M^c, d_M^c] &= [2, 2]. \end{aligned} \quad (16)$$

Therefore, the order for the desired discrete-time closed-loop TF from (15) using the ZOH method is

$$[n_a, n_b] = [n_A^d, n_B^d] = [3, 4]. \quad (17)$$

Here the superscripts c and d signify continuous-time and discrete-time TFs, respectively, and the subscripts A and B signify the numerator and denominator polynomials of the closed-loop TF $B(q)/A(q)$ in (11).

3.2.2 Deduction of plant TF

The discrete-time plant model was obtained from the closed-loop TF identified in Subsection 3.2.1 as follows. Rearranging (15), we get the identity

$$G(q) = T(q)[M(q) - M(q)T(q)]^{-1}. \quad (18)$$

Using (11) with the closed-loop TF orders (17) and the relation (18), we obtain the high-order identified plant TFs. For the purpose of order reduction and analysis of the frequency-domain behavior of the identified plant model, the TF was converted to a continuous-time model. The high-order identified continuous-time TF for x , for example, is given by (19) below.

$$G_{xx}(s) = 3.1435 \times 10^{-5} \frac{N(s)}{D(s)}, \quad (19)$$

where

$$N(s) = \begin{bmatrix} s^2 (s + 4014)^2 \\ \cdot (s^2 + 335s + 1.2750 \times 10^6) \\ \cdot (s^2 + 6102s + 1.1090 \times 10^7) \\ \cdot (s + 13123)(s^2 - 9947s + 3.4330 \times 10^7) \end{bmatrix} \quad (20)$$

and

$$D(s) = \begin{bmatrix} (s - 54.6250)(s + 76.9111) \\ \cdot (s)(s + 11.4763)(s + 4014)(s + 4042) \\ \cdot (s^2 + 335s + 1.2750 \times 10^6) \\ \cdot (s^2 + 6102s + 1.1090 \times 10^7) \\ \cdot (s^2 + 2450s + 4.2460 \times 10^6) \end{bmatrix}. \quad (21)$$

The pole-zero map of this TF is shown in Fig. 6(a), and the magnitude of the TF is shown in Fig. 7(a) with a thick dashed line.

3.2.3 Order reduction

Although the identified TF (19) is 12th order, there are several pole-zero pairs at the identical locations on the pole-zero map as seen in Fig. 6(a) because of the way in which the TF was deduced in Subsection 3.2.2. Consider, for instance, a single-input-single-output (SISO) plant with the identified plant TF given by (18). The denominator polynomial of $T(q)$ appears in both the numerator and the denominator of $G(q)$ after simplification and hence results in pole-zero pairs at identical locations. The polynomials $(s^2 + 335s + 1.2750 \times 10^6)$ and $(s^2 + 6102s + 1.1090 \times 10^7)$ in (19) result from such mathematical manipulation and hence are spurious in nature. The cancellation of these spurious pole-zero pairs reduces the order of the plant significantly.

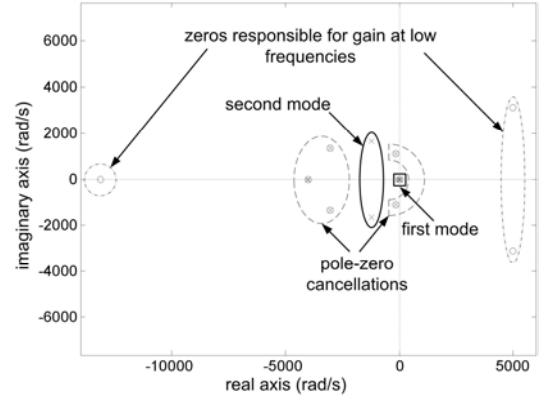
The order may be further reduced by eliminating the zeros which are at frequencies much higher than the closed-loop bandwidth and hence would not affect the system dynamics significantly. Appropriate adjustments need to be made in the TF magnitude.

Finally, with the remaining poles and zeros, the dynamics of the system can be divided into two modes—the first mode is the slowest and very close to a double-integrator. This mode is of greatest interest in the design of a controller since it represents the rigid-body dynamics of the maglev positioner. The second mode corresponds to the mechanical vibrations of the maglev positioner with a resonant frequency around 325 Hz and can be ignored in the plant model since the designed controller has a control bandwidth of about 110 Hz and is not expected to excite this high-frequency mode.

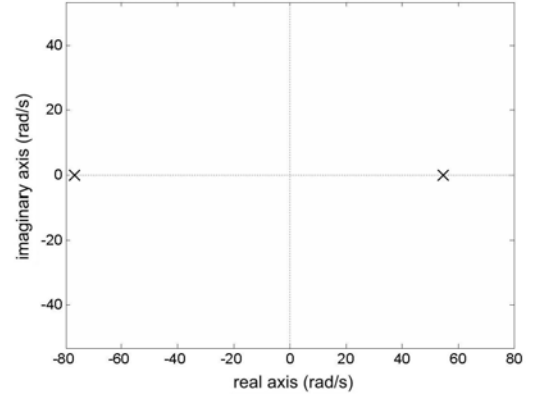
3.3. Reduced-order identified TF models

With the order reduction described in Subsection 3.2, the order of the plant TF becomes $\left[n_G^c, d_G^c \right]_{iden} = [0, 2]$.

The reduced-order TF fit so obtained is shown in the Fig. 7(a) with a thick solid line. It matches with the identified TF in the frequency range of [20, 300] Hz (within an error of 1%. This error is calculated as $\varepsilon = |(P_i - P_r)/P_i|$, where P_i and P_r are the magnitudes of the identified plant TFs and their corresponding reduced-order fits. The corresponding pole-zero map is shown in the Fig. 6(b). The TFs for the coupling terms are obtained in a similar manner and are shown in Figs. 7(b) and 7(c). These identified continuous-time TFs are given by



(a) The identified full-order TF in x .



(b) The identified reduced-order TF in x .

Fig. 6. Pole-zero maps.

$$G_{xx}(s) = \frac{3.1845}{(s - 54.62)(s + 76.91)}, \quad (22a)$$

$$G_{xy}(s) = \frac{42.4017}{(s + 13.83)(s^2 + 219.40s + 1.98 \times 10^6)}, \quad (22b)$$

$$G_{x\phi}(s) = \frac{0.4266(s - 6977.00)}{(s - 9.74)(s^2 + 451.50s + 1.17 \times 10^6)}, \quad (22c)$$

$$G_{yy}(s) = \frac{3.1623}{(s - 82.21)(s + 76.91)}, \quad (23a)$$

$$G_{yx}(s) = \frac{114.9298}{(s + 105.91)(s^2 + 131.00s + 1.09 \times 10^6)}, \quad (23b)$$

$$G_{y\phi}(s) = \frac{964.3725}{(s + 322.80)(s^2 + 65.59s + 7.29 \times 10^5)}, \quad (23c)$$

$$G_{\phi\phi}(s) = \frac{1530.1985}{(s - 86.73)(s + 76.91)}, \quad (24a)$$

$$G_{\phi x}(s) = \frac{0.1411(s - 934.60)}{(s + 76.91)(s^2 + 586.20s + 2.53 \times 10^5)}, \quad (24b)$$

$$G_{\phi y}(s) = \frac{0.9065}{(s + 76.91)(s + 315.60)}. \quad (24c)$$

The right-half-plane poles identified in (22a), (23a), and (24a) reflect the maglev system's open-loop instability due to the negative spring constants of the magnetic origin. The frequency responses of the identified plant models are represented in Figs. 7(a), 7(e), and 7(i). These

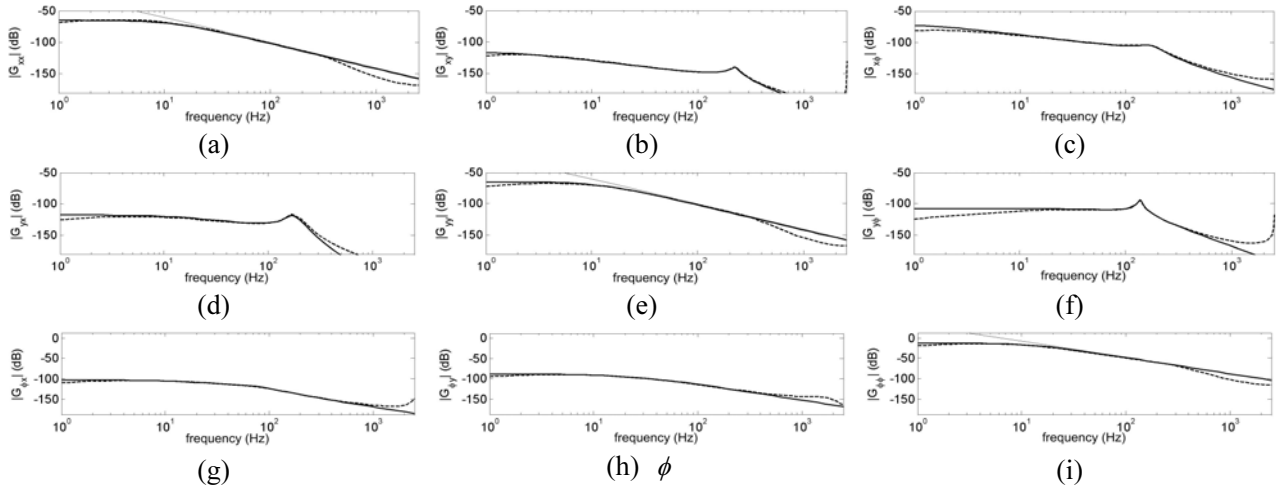


Fig. 7. Analytical plant TFs (thin solid lines), identified plant TFs (thick dashed lines) and reduced-order fit (thick solid lines) from (a) x to x , (b) x to y , (c) x to ϕ , (d) y to x , (e) y to y , (f) y to ϕ , (g) ϕ to x , (h) ϕ to y , and (i) ϕ to ϕ .

plots show the analytical plant models (thin solid lines) from (10), the identified plant models (thick dashed lines) from (19) (for x) using the closed-loop system identification from the input-output time sequences, and the reduced-order fits (thick solid lines) from (22)-(24). From these frequency responses, it is apparent that there are certain mismatches between the analytical and identified models. The mismatch in the low-frequency range is due to the fact that the plant TFs are indeed not of pure double-integrators but consist of two real poles at different locations with the existence of magnetic springs in the actuators. In the high-frequency range, the mismatch may be due to unmodeled dynamics. However, in the frequency range of interest, [20, 300] Hz, the two models exhibit an almost perfect match. In addition to this match in the frequency domain, time-domain dynamic behaviors, particularly the transient response, of the reduced-order TFs are also important.

Other identified TFs of interest are the off-diagonal ones in (8) that may be used to reduce the dynamic coupling among the axes. These TFs are also presented in Figs. 7(b), 7(c), 7(d), 7(f), 7(g), and 7(h). The orders of the reduced-order TFs are identically chosen to be 3 for all the coupling terms for the consistency and ease of controller design using this information. A comparison between the TFs $G_{xy}(s)$ and $G_{yx}(s)$ shows that the peak value of the plot is greater for $G_{yx}(s)$, particularly in the frequency range of [50, 250] Hz. Similarly, comparing $G_{x\phi}(s)$ and $G_{y\phi}(s)$, the magnitude of the $G_{x\phi}(s)$ is greater. This is in agreement with the response plots in Figs. 5(a), 5(b), and 5(c) discussed earlier in Subsection 3.1.

3.4. Model validation

In order to validate the model identification discussed above and demonstrate its feasibility in real-life applications, a MIMO control was designed using identified plant and coupling TFs models. Unlike the decoupled control with the linearized plant TFs about an operating point as given by (10), this MIMO control uses

outputs from all three modes and calculates the controller input for the plant as well as the coupling TFs. The closed-loop system response with the designed controller is therefore expected to meet the objectives outlined in Section 1. A detailed discussion of the MIMO control design is beyond the scope of this paper as it mainly focuses on the identification of the unstable multivariable systems. For the sake of completeness, however, we present some experimental results that validate the accuracy of the identified models.

The first result shown in Fig. 8 demonstrates the effect of the identified model on better and more accurate controller design. This figure shows the plant input and closed-loop responses to a 100- μm reference step of the actual controlled system with controllers designed using identified model (22) and analytical model (10). It also shows the simulated response using identified plant TF models. It is apparent from the figure that the identified model gives a closer match with the simulated results and hence is more reliable. The small mismatch between the simulated response and the response using the identified TF model is due to the fact that the simulation results do not incorporate the coupling terms. On the other hand, the actuator input computed by the controller as shown in the figure includes coupling terms from the other two outputs as well.

Another set of experiments was conducted with an objective to demonstrate the increased working space and linearity achieved with the use of identified models. Fig. 9 shows the coupled closed-loop system responses in y and ϕ with a 100- μm step in x . However, unlike Fig. 8 where a step was commanded about the operating point $x = 0$, the step command here was given at $x = 2.9$ mm. Because of the nonlinearities present in the actuators that increase very rapidly with the increase in the distance between the coil and the magnet, a deviation of 2.9 mm from the operating point is large enough to make significant changes in the plant output. This is apparent from Fig. 9. Although the responses in x is almost similar to Fig. 8, the coupling with the controllers

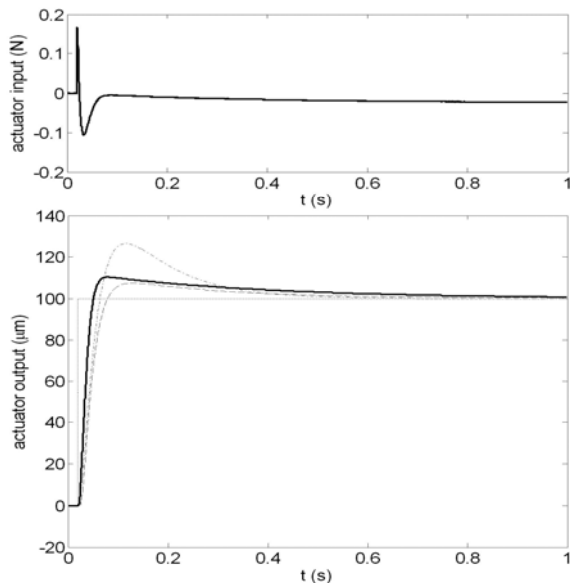


Fig. 8. Experimental validation of the identified plant TFs—Plant input and closed-loop step responses of the actual controlled system with controllers designed using identified model (thick solid line) and analytical model (thin solid line). Simulated response (dashed line) shows a closer match with the actual system response. Dotted line shows reference input signal.

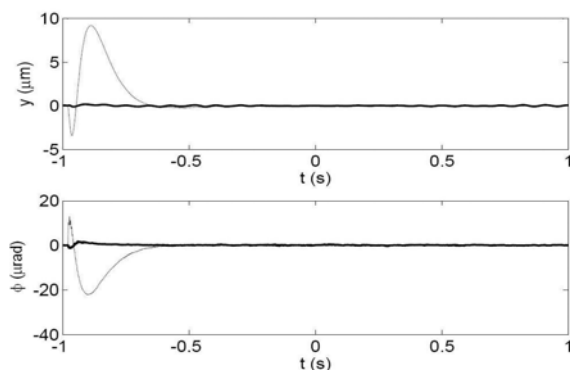


Fig. 9. Response of the system to a $100\text{-}\mu\text{m}$ step at an operating point 2.9 mm away from the point of linearization with decentralized controllers designed using linearized analytical plant models ignoring coupling TFs (thin lines) and with MIMO control designed with identified plant and coupling TFs (thick lines).

designed using analytical models increased significantly as we moved away from the operating point about which the system was linearized. This is due to the fact that there were no coupling TFs to capture and correct the cross-axial components in real time. With the use of identified coupling TFs in the design of MIMO control, this problem was taken care of. Note that similar coupling compensation can also be achieved through nonlinear feedback linearization if we have perfect knowledge of the actuator nonlinearities at all frequencies. However, even in a relatively simple system,

modeling such nonlinearities accurately can be quite challenging. For more complex systems, this may not be feasible. However, closed-loop model identification offers an alternate and better option to identify and compensate for such nonlinear behavior present in the system—whether stable or unstable—by capturing the actual plant dynamics.

4. CONCLUSIONS

This paper proposed an approach for multivariable system identification in the closed-loop framework. In this approach, the dynamics of an unstable system is represented using a TF matrix in the standard form used in any traditional input-output identification method, but with open-loop TFs replaced with closed-loop TFs and with known controller structures. This model structure is capable of identifying a very large class of multivariable systems found in practical applications. The system identification problem was considered as the problem of simultaneously estimating the parameters of all three plant TFs and six coupling TFs of the TF matrix. An order-reduction algorithm was used to reduce the high-order identified TFs to predetermined fixed-structure TFs, which facilitate the subsequent controller design.

Experimental results on the frequency-domain validation of the identified models were presented for all nine TFs and compared with their analytical and full-order counterparts. From these results, the reduced-order models were found to have a significantly close match with the identified results, with errors less than 1% in the frequency range of $[20, 300]$ Hz. Step responses with the controllers designed with analytical and reduced-order identified TFs were also presented in this paper and compared to check for any missing transient dynamics and to discuss the improvements in the controller design with the identified models. The entire analysis was performed using difference equations to avoid any digitization error from the continuous-to-discrete-time conversion. The continuous-time analyses with Bode plots and pole-zero maps were performed to interpret the physical meaning of the identified models and to demonstrate the effectiveness of the closed-loop system-identification and order-reduction algorithms. Step responses with the controllers designed using identified TFs were also presented to demonstrate the effectiveness of the developed closed-loop identification method in meeting all the key objectives. The identified TF models resulted in a reduction in cross-axial coupling from $9.213\ \mu\text{m}$ to $0.911\ \mu\text{m}$ in translation and from $22.03\ \mu\text{rad}$ to $1.353\ \mu\text{rad}$ in rotation; large range motion capability with a travel range of $\pm 2.9\text{ mm}$; and improved robust stability.

REFERENCES

- [1] S. Verma, H. Shakir, and W.-J. Kim, "Novel electromagnetic actuation scheme for multi-axis nanopositioning," *IEEE Trans. on Magnetics*, vol. 42, no. 8, pp. 2052-2062, Aug. 2006.
- [2] S. Earnshaw, "On the nature of the molecular forces which regulate the constitution of the luminiferous

ether," *Trans. of the Cambridge Philosophical Society*, vol. 7, pp. 97-112, 1842.

- [3] X. Bombois, M. Gevers, and G. Scorletti, "Open-loop versus closed-loop identification of Box-Jenkins models: a new variance analysis," *Proc. 44th IEEE Conf. on Decision and Control*, pp. 3117-3122, Dec. 2005.
- [4] L. Sun, H. Ohmori, and A. Sano, "Direct closed-loop identification of magnetic suspension system," *Proc. IEEE Intl. Conf. on Control Applications*, vol. 1, pp. 749-754, Aug. 1999.
- [5] F. R. Hansen and G. F. Franklin, "On a fractional representation approach to closed-loop experimental design," *Proc. American Control Conference*, pp. 1319-1320, 1988.
- [6] S. K. Kuo, X. Shan, and C. H. Menq, "Large travel ultra precision x-y-z motion control of a magnetic-suspension stage," *IEEE Trans. on Mechatronics*, vol. 8, no. 3, pp. 334-341, Sep. 2003.
- [7] S. Dejima, W. Gao, K. Katakura, S. Kiyono, and Y. Tomita, "Dynamic modeling, controller design and experimental validation of a planar motion stage for precision positioning," *Precision Engineering*, vol. 29, no. 3, pp. 263-271, Jul. 2005.
- [8] E. Villota and S. Jayasuriya, "Model based control of a multidimensional positioning system - a comparison of controller designs with experimental validation," *Proc. American Control Conference*, Portland, OR, pp. 1365-1370, Jun. 2005.
- [9] C. E. Lin and H. L. Jou, "Force model identification for magnetic suspension systems via magnetic field measurement," *IEEE Trans. on Instrumentation and Measurement*, vol. 42, no. 3, pp. 767-771, Jun. 1993.
- [10] K. Nakashima, T. Tsujino, and T. Fujii, "Multivariable control of a magnetic levitation system using closed loop identification and \mathcal{H}_∞ control theory," *Proc. 35th IEEE Conf. on Decision and Control*, vol. 4, Kobe, Japan, pp. 3668-3673, Dec. 1996.
- [11] U. Forssell and L. Ljung, "Closed-loop identification revisited," *Automatica*, vol. 35, no. 7, pp. 1215-1241, Jul. 1999.
- [12] P. M. J. Van den Hof and R. J. P. Schrama, "Identification and control—Closed-loop issues," *Automatica*, vol. 31, no. 12, pp. 1751-1770, Dec. 1995.
- [13] H. Shakir, W.-J. Kim, and S. Verma, "System identification and optimal control of a 6-DOF magnetic levitation stage with nanopositioning capabilities," *Proc. of the ASME International Mechanical Engineering Congress and Exposition*, Paper No. 60507, Nov. 2004.
- [14] R. Pintelon and J. Schoukens, "Box-Jenkins identification revisited Part I: Theory," *Automatica*, vol. 42, no. 1, pp. 63-75, Jan. 2006.
- [15] L. Ljung, *System Identification: Theory for the User*, 2nd ed., Prentice-Hall, Upper Saddle River, NJ, 1999.
- [16] R. Pintelon and J. Schoukens, *System Identification: A Frequency Domain Approach*, IEEE Press, 2001.



Huzefa Shakir received his B.Tech. (Hons) in Mechanical Engineering from Indian Institute of Technology, Kharagpur, India, in 2000, and his Ph.D. degree in Mechanical Engineering from Texas A&M University, College Station, in 2007. Since 2007, he has been working as senior scientist with the applied research division of Halliburton. He has

worked as Assistant Manager in Suzuki Motor Corporation India for two years following receipt of the Bachelor's degree. His expertise are in the areas of design and control of precision positioning systems, microelectromechanical systems, high-temperature high-pressure sensors, electromagnetic telemetry, and precision wellbore placement.

Dr. Shakir has published a monograph and more than twelve other publications in numerous journals and conferences proceedings. He was the recipient of the best paper award in the American Control Conference 2005, International Texas Public Education Grant 2006, and Fellowship at the Center for Teaching Excellence, Texas A&M University. His biographical entry has been published in the prestigious Marquis' Who's Who in America® 2010 and 2011 editions for his outstanding achievements in the field of engineering. He is a member of Institute of Electronics and Electrical Engineers (IEEE), American Society of Mechanical Engineers (ASME), Society of Petroleum Engineers (SPE) and The Honor Society of Phi Kappa Phi. He also serves on the Industry Steering Committee on Wellbore Survey Accuracy (ISCSWA).



Won-jong Kim received his B.S. (summa cum laude) and M.S. degrees in Control and Instrumentation Engineering from Seoul National University, Seoul, Korea, in 1989 and 1991, respectively, and his Ph.D. degree in Electrical Engineering and Computer Science from the Massachusetts Institute of Technology (MIT), Cambridge, in 1997. Since 2000,

he has been with the Department of Mechanical Engineering, Texas A&M University (TAMU), College Station, where currently he is an Associate Professor and the Holder of the Dietz Career Development Professorship II. After the Ph.D. degree, he was with SatCon Technology Corporation, Cambridge, MA, for three years. His current research interests include the analysis, design, and real-time control of mechatronic systems, networked control systems, and nanoscale engineering and technology. He is the holder of three U.S. patents on precision positioning systems.

He was the recipient of Korean Institute of Electrical Engineers' Student Paper Contest grand prize in 1988, Samsung Electronics' Humantech Thesis gold prize for his MIT dissertation in 1997, the NASA Space Act Award in 2002, and the 2005 Professional Engineering Publishing Award for the best paper published in 2004 in *Journal of Engineering Manufacture*. He was also a semifinalist of the National Institute of Standards and Technology (NIST)'s Advanced Technology Program competition in 2000. He was appointed a Select Young Faculty Fellow by TAMU College of Engineering and the Texas Engineering Experiment Station twice in 2003 and 2005. He received the BP Teaching Excellence Award by TAMU College of Engineering in 2006. He is Fellow of ASME, Senior Member of IEEE, and Member of Pi Tau Sigma. Prof. Kim is Technical Editor of IEEE/ASME Transactions on Mechatronics, ASME Journal of Dynamic Systems, Measurement and Control, and International Journal of Control, Automation, and Systems.